A Comparison of Cryogenic-Cooled and Superconducting Electrical Machines

A Comparison of Cryogenic-Cooled and Superconducting Electrical Machines

Marco Biasion, *Student Member, IEEE*
Politecnico di Torino
Dipartimento Energia
Torino, Italy
marco.biasion@polito.it

João F. P. Fernandes, *Member, IEEE*
IDMEC, Instituto Superior Técnico
University of Lisbon
Lisbon, Portugal
joao.f.p.fernandes@tecnico.ulisboa.pt

Paulo José da Costa Branco, *Member, IEEE*
IDMEC, Instituto Superior Técnico
University of Lisbon
Lisbon, Portugal
pbranco@tecnico.ulisboa.pt

Silvio Vaschetto, *Senior Member, IEEE*
Politecnico di Torino
Dipartimento Energia
Torino, Italy
silvio.vaschetto@polito.it

Andrea Cavagnino, *Fellow, IEEE*
Politecnico di Torino
Dipartimento Energia
Torino, Italy
andrea.cavagnino@polito.it

Alberto Tenconi, *Senior Member, IEEE*
Politecnico di Torino
Dipartimento Energia
Torino, Italy
alberto.tenconi@polito.it

***Abstract*—This paper compares the steady-state operation of air-cooled, cryogenic-cooled and superconducting induction machines. The aim is to investigate the impact of a very low temperature and the influence of a superconducting rotor cage on the performances of standard designed, air-cooled machines. The research work includes a review of the state of the art of cryogenic-cooled and superconducting induction machines for various applications. The performances of the machines are assessed analytically by solving the single-phase equivalent circuit and considering the influence of the temperature, the skin-effect and the nonlinear behavior of superconductors. The analytical results are validated by experiments on a fractional kilowatt induction motor. The experimental activities include the characterization of the core losses at cryogenic temperature.**

Keywords—Electrical machines, induction machines, cooling, superconductors, cryogenics, core losses, modeling, testing.

I. Introduction

Induction machines (IMs) have been considered the workhorse of industry because of their inherent low cost, high reliability, robustness and technology maturity compared to other machine topologies. They have been employed in many applications including some non-conventional ones, like cryogenic pumps. The operation of the machine submerged in a cryogenic liquid at very low temperature allows superior cooling of the active parts. This results in a higher specific torque, lower Joule losses and improved efficiency compared to air-cooled machine designs of the same size [1]. Moreover, problems associated with conventional insulating materials operated in air, such as partial discharge, thermal life and oxidation, can be eliminated using tailored solutions [2]. The operation of the machine at cryogenic temperatures also allows investigating the use of superconductors (SCs) in place of conventional conducting materials for the machine windings. Specifically, by using a superconducting rotor cage the machine can provide unique electromechanical characteristics because of the peculiar electric behavior of SCs [3] – [5].

Cryogenic-cooled IMs have found applications in missile cryogenic propellant apparatuses operating with liquid hydrogen at -253 °C [1]. They have also been used in liquefied natural gas (LNG) pump applications operating at -161 °C [6], [7]. Their use with liquid nitrogen (LN_2) is also quite common, especially for testing purposes since LNG is highly flammable [6].

Superconducting IMs have been analyzed for a long time since the use of SCs in power equipment was possible. Among the different studies, [8] and [9] described their operating principle expressing excitement and concerns about their success, respectively. Much study in recent years has focused on investigating superconducting IMs using High Temperature Superconducting (HTS) materials. For instance, different research activities aimed at demonstrating the potentials of this machine topology as traction motor for transportation means such as trains, buses, trucks and automobiles [10], [11].

The performance comparison between cryogenic-cooled and air-cooled conventional IMs was carried out in [12]. A similar study considering superconducting and air-cooled IMs was presented in [13]. Nevertheless, little attention has been paid to a detailed performance investigation of cryogenic-cooled, superconducting and air-cooled IMs all together.

The present paper compares the performance of cryogenic-cooled and superconducting IMs with those of air-cooled designs. First, a brief review of the state of the art of cryogenic-cooled and superconducting IMs is provided. A 90 W and a 15 kW three-phase air-cooled industrial motors are taken as the reference for the study. Their steady-state performances are investigated theoretically with the single-phase equivalent circuit, considering a cryogenic cooling and a superconducting rotor cage. Experimental results on the 90 W machine with a cryogenic cooling are presented to prove the effectiveness of the proposed methodology. The superconducting solution is also assessed analytically. The study includes experimental investigations on the core losses at cryogenic temperature.

II. State of the Art

A. Cryogenic-cooled IMs

Electrical machines for cryogenic applications can be operated totally submerged in a very low temperature environment. Cryogenic-cooled IM refers to devices employing conventional conducting materials and with all their active parts wetted by a cryogenic fluid. The magnetic core is normally manufactured using SiFe alloys. Figure 1 illustrates the cross-section of a cryogenic-cooled IM for LNG pumps [7].

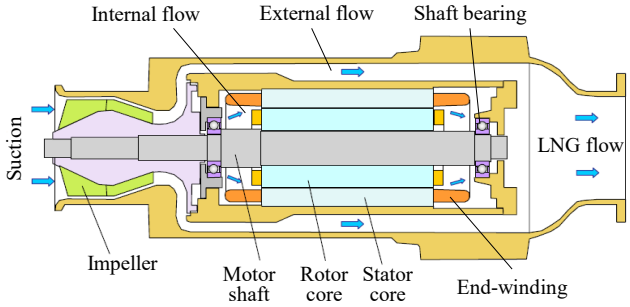

Fig. 1. Submerged pump assembly for LNG applications using a cryogenic-cooled induction machine (adapted from [7]).

The internal flow circulates mainly through the airgap of the machine and does not only serve as a coolant, but it also lubricates the shaft bearings. The external flow is the pumped one at higher pressure.

The operation of the machine in the cryogenic environment has remarkable consequences on its performances. An almost tenfold reduction in the electrical resistivity of copper conductors allows to increase the electrical loading of the machine [14]. This fact, along with the superior heat extraction capability of cryogenic fluids, allows to enhance the torque density by reducing the machine dimensions compared to an air-cooled design of the same rating [7]. Reference [12] showed the possibility to design a cryogenic-cooled IM providing the desired torque with an almost 40% reduction in volume compared to an equivalent air-cooled design. However, for a given magnetic loading, core losses are generally higher with respect to those of air-cooled machines since the electrical conductivity of laminations increases at lower temperature [14]. Furthermore, the presence of the fluid in the airgap causes a remarkable increase in friction losses compared to an air-cooled machine [14].

B. Superconducting IMs

Superconducting materials in the form of tapes and bulks can replace conventional conducting materials in the fabrication of windings, permanent magnets and flux shields for AC and DC electrical machines. A detailed review on superconductivity and its application to electrical machines was provided by the authors in [3].

Figure 2 shows the electric field E versus current density J characteristic of a HTS material at constant temperature and magnetic field. The electrical resistivity of SCs is highly nonlinear: its value in the superconducting state is close to zero and varies of several orders of magnitude when entering the dissipative state. The critical current density J_c identifies the transition from the superconducting to the dissipative state and changes from material to material. It is determined experimentally and defined when the electric field within the superconductor is equal to the characteristic field E_0. For HTS materials, E_0 is normally set to the standard value of 1 µV/cm. The E-J characteristic of HTS materials at constant temperature and magnetic field can be described analytically using a power law, as shown in Fig. 2.

The manufacturing, the operating principle and the control strategies for superconducting IMs have been analyzed extensively in the literature so far [15] – [18]. In those studies, the machine was often referred as induction/synchronous motor.

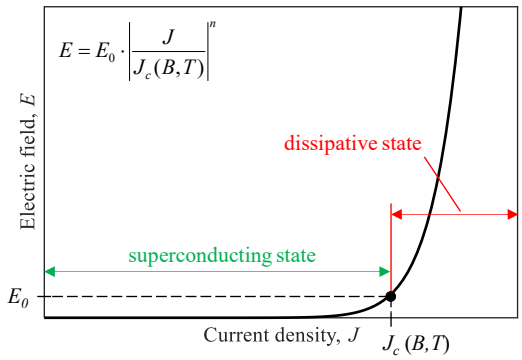

Fig. 2. Electric field vs. current density characteristic of a HTS material at constant temperature and constant magnetic field.

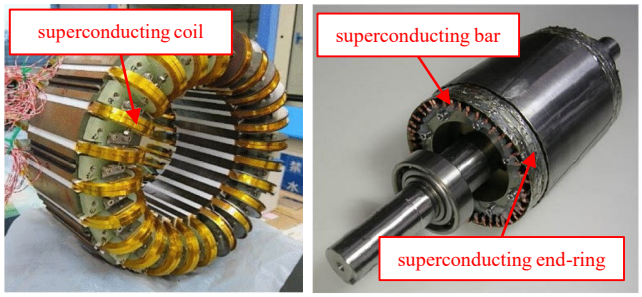

(a) (b)

Fig. 3. Superconducting IMs. (a) 50 kW induction/synchronous machine prototype equipped with superconducting ring coils on the stator (adapted from [5]). (b) Superconducting rotor cage of a 1.5 kW induction/synchronous machine prototype (adapted from [17]).

Indeed, it was reported that an induction machine with a superconducting rotor cage can provide an electromagnetic torque when rotating at the synchronous speed. The stator winding can be manufactured either using SCs or conventional copper conductors.

The operating principle of a superconducting induction machine relies on the nonlinear behavior of SCs as well as the flux-trapping phenomenon [17].

Considering a line-connected superconducting IM, at the startup phase high rotor currents at the line frequency cause the SCs to operate in their dissipative state and the rotor cage to exhibit a high electrical resistance. The machine is therefore able to provide a starting torque. While accelerating towards the synchronous speed, the frequency and the magnitude of the rotor currents decrease. As soon as the SCs enter the superconducting state, their resistivity drops to almost zero. Consequently, the rotor flux linkage is trapped within the superconducting cage, which acts as a field source analogous to permanent magnets. The superconducting IM can provide a temporary output torque at the synchronous speed, as it will be articulated in Section III.

Figure 3a shows the ring winding configuration of the superconducting stator of a 50 kW machine prototype [5]. This arrangement of SCs was necessary because of their limited bending radius. Figure 3b illustrates the superconducting rotor cage of the 1.5 kW machine prototype presented in [17]. The superconducting rotor bars were welded to the end-rings. This process introduced a small additional resistance contribution to the rotor cage. Both the machine prototypes demonstrated their capability to operate in the synchronous mode at partial load or at full load.

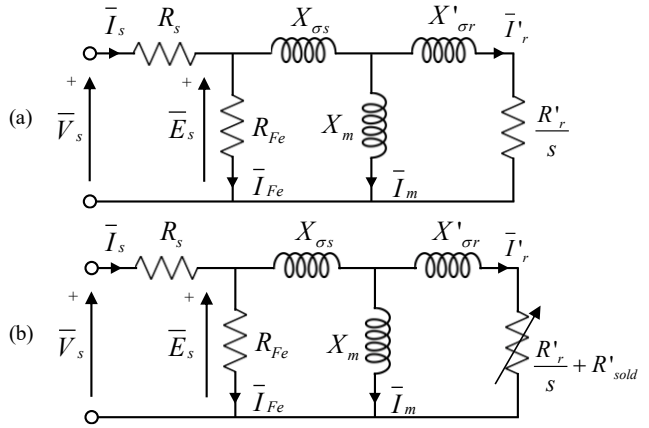

Fig. 4. Single-phase equivalent circuit. (a) Circuit used for the reference (REF) and the cryogenic-cooled (CRYO) machine concepts. (b) Circuit used for the machine concept with the superconducting rotor cage (SC).

III. The Methodological Approach

The investigations involved comparing the steady-state performance of cryogenic-cooled and superconducting IMs to conventional air-cooled designs. Two different air-cooled industrial motors were taken as the reference for the study: a 15 kW, 400 V, 50 Hz, four-pole machine and a 90 W, 40 V, 50 Hz, four-pole machine, respectively.

The characteristics of the analyzed air-cooled (REF), cryogenic-cooled (CRYO) and superconducting (SC) IMs are reported in Table I. The CRYO and the SC IMs were investigated considering their operation at the boiling point of LN_2 at -196 °C (77 K). The BSCCO-2223 HTS tapes considered for the analysis of the superconducting induction machine concept were described in [3]. They can be operated with LN_2 since their critical temperature T_c is of ~ 110 K. The machine concepts REF, CRYO and SC featured the same active volume and the same conventional stator winding configuration.

The performance comparison was based on analytical calculations performed considering the single-phase equivalent circuit depicted in Fig. 4. Also, some experimental tests were carried out, as it will be described in Section IV. Figure 4a shows the circuit used to analyze the air-cooled (REF) and the cryogenic-cooled (CRYO) machines, while Fig. 4b depicts the circuit used to model the superconducting (SC) machine. Here, the use of a variable rotor resistance was necessary because of the nonlinear resistivity of HTS materials. Indeed, the value for the equivalent rotor-phase resistance R'_r depends on the actual current density in the rotor cage, so that $R'_r = f(J_r)$.

When employing SCs it is no longer possible to manufacture a die-cast rotor cage. Therefore, solder is commonly used to weld together the rotor bars and the end-rings. The soldering resistance R'_{sold} accounts for this additional contribution and its value, converted to the stator side, was set to 10^{-5} Ω [19].

In Section II.B it was pointed out that the superconducting IM can provide an output torque at the synchronous speed. However, the rotation at the synchronous speed is only temporary. Indeed, the rotor flux linkage cannot be maintained constant since the rotor currents decay in time following a first-order exponential behavior, governed by the rotor's time constant. The resistive contribution to the time constant is mainly due to the soldering resistance R'_{sold}, which is higher than the resistance of the SCs operating in their superconducting state.

TABLE I. Description of the Analyzed Machines.

Machine concept	Operating temperature	Materials		
		Rotor cage	*Stator winding*	*Iron core*
REF	80 °C (air-cooled)	Aluminum die-cast	Copper distributed	SiFe alloys
CRYO	-196 °C (LN_2 cooling)			
SC	-196 °C (LN_2 cooling)	BSCCO-2223 HTS tapes		

TABLE II. Influence of the Temperature and the Skin Effect on the Parameters of the Single-Phase Equivalent Circuit.

Parameter	Temperature	Skin effect
Stator resistance, R_s	✓	negligible
Stator leakage reactance, $X_{\sigma s}$	not applicable	negligible
Eq. iron loss resistance, R_{Fe}	experiments	not applicable
Magnetizing reactance X_m	not applicable	negligible
Rotor leakage reactance $X'_{\sigma r}$ (REF, CRYO)	not applicable	✓
Rotor-phase resistance R'_r (REF, CRYO)	✓	✓
Rotor parameters R'_r, $X'_{\sigma r}$ (SC)	dedicated model	

In other words, the machine can rotate at steady state as a conventional induction motor featuring very small rotor resistance ($R'_r \approx R'_{sold}$) and slip values. For these reasons, only the asynchronous operation of superconducting machines was analyzed in this paper.

The parameters of the equivalent circuits shown in Fig. 4 were determined analytically following the approach presented in [20], [21]. The calculation of the rotor resistance of the SC machines was performed adapting the methodology presented in [20]. In detail, the analytical description of SCs was included using the power law shown in Fig. 2.

A different operating temperature of the machine influences the electrical conductivity of materials. Consequently, the *dc* value of the electrical resistivity of the conductors as well as the electrical resistivity of the iron core change accordingly. The influence of the skin effect is also different when the operating temperature changes. The variation of the parameters of the equivalent circuit due to the above-mentioned effects is summarized in Table II. At a constant supply frequency, the value for the magnetizing reactance X_m depends on the arrangement of the stator winding and the geometry of the machine core, which remained the same throughout the study. The value for the stator leakage reactance $X_{\sigma s}$ does not depend on the operating temperature, but it may depend on the skin effect. However, because of a low supply frequency and a random-wound configuration of the stator winding, the influence of the skin effect on both $X_{\sigma s}$ and R_s is generally negligible. The variation of the stator resistance R_s with the temperature was considered by correcting the value of the electrical resistivity of copper from room to cryogenic temperature. From 80 °C to -196 °C the *dc* value for the resistivity of copper decreases of about 88%. The variation of the iron losses with the temperature, i.e., the parameter R_{Fe}, was verified experimentally. The results will be described in Section IV.A. The computation of the rotor parameters $X'_{\sigma r}$ and R'_r for the CRYO and SC machines is described hereafter.

A. CRYO machine concept: rotor resistance

The equivalent rotor-phase resistance R_r can be expressed by (1), as shown in [20]. In this equation, K_R is the skin-effect coefficient for the rotor bar resistance, $R_{b,DC}$ is the *dc* resistance of the rotor bar, R_a is the *dc* resistance of the end-ring, N_{bars} is the number of bars of the rotor cage and β_r is the angle between two adjacent rotor bars. The resistance R_r is a function of the operating temperature θ because of the variation of K_R, $R_{b,DC}$ and R_a with the temperature. The skin effect on the end-ring was assumed negligible in the study.

$$R_r(\theta) = K_R(\theta) \cdot R_{b,DC}(\theta) + \frac{2R_a(\theta)}{4N_{bars}\,\mathrm{sen}^2\left(\frac{\beta_r}{2}\right)}. \quad (1)$$

The value for the equivalent rotor-phase resistance R_r was calculated for the reference machines (REF) and validated experimentally by performing the locked-rotor test. Since the cryogenic-cooled machines (CRYO) maintained the same structure as the reference machines, the parameter R_r at cryogenic temperature was easily determined by correcting the value of the electrical resistivity of aluminum from 80 °C to -196 °C. In this way, both the *dc* resistance and the skin effect coefficient were modified. The rotor resistance was converted to stator side (R'_r) using the parameter K_{RS} described in (2) [20]. Z_{ph} is the number of conductors in series per phase of the stator winding and $k_{w,1}$ is the fundamental winding factor of the stator winding.

$$R'_r = K_{RS} \cdot R_r = \frac{3}{N_{bars}}\left(Z_{ph} \cdot k_{w,1}\right)^2 \cdot R_r. \quad (2)$$

B. CRYO machine concept: rotor leakage reactance

The rotor leakage reactance $X_{\sigma r}$ is composed of different contributions as shown in (3). In detail, X_{leak_airgap} represents the contribution due to the slotting effect and the distribution of the stator winding along the circumference of the airgap, X_{end_ring} represents the leakage reactance of the end-ring, X_{slot_leak} represents the rotor slot leakage reactance and $X_{leak,incl\_r}$ describes the influence of the skewing of the rotor bars [20]. The rotor slot leakage component X_{slot_leak} is influenced by the skin effect, which also depends on the operating temperature θ. The skin effect on the end-ring was disregarded [21]. The reactance $X_{\sigma r}$ was converted to the stator side using the K_{RS} factor introduced in (2), where $X'_{\sigma r} = K_{RS} \cdot X_{\sigma r}$ [20].

$$X_{\sigma r} = X_{leak\_airgap} + X_{end\_ring} + X_{slot\_leak}(\theta) + X_{leak,incl\_r}. \quad (3)$$

The rotor slot leakage component X_{slot_leak} can be written as indicated in (4), highlighting the skin-effect coefficient $K_L(\theta)$. The *dc* value for the slot leakage reactance $X_{slot\_leak\_DC}$ can be computed starting from the rotor slot geometry [20].

$$X_{slot\_leak}(\theta) = K_L(\theta) \cdot X_{slot\_leak\_DC}. \quad (4)$$

The rotor leakage reactance $X_{\sigma r}$ was calculated for the reference machines (REF) and validated experimentally by performing the locked-rotor test. By assuming that among all the terms reported in (3) only the slot leakage contribution changes with the temperature, its value was corrected simply modifying the skin-effect coefficient from 80 °C to -196 °C.

C. SC machine concept: rotor leakage reactance

The SC machine concept was investigated considering the BSCCO-2223 HTS material. The cross-sectional dimensions of a single tape were 4.1 mm × 0.28 mm. Two tapes in parallel configuration were considered for each of the rotor bars and the end-rings. Their narrow thickness in addition to a low operating frequency of the machine, even in the locked-rotor condition, allowed to neglect the influence of the skin effect in the superconducting tapes. Therefore, K_L in (4) was set equal to one. The rotor leakage reactance of the SC machine concept $X_{\sigma r,SC}$ was computed as reported in (5). It can be concluded that the value for $X_{\sigma r,SC}$ does not depend on the operating temperature of the machine. Also in this case, the value $X_{\sigma r,SC}$ was converted to the stator side with the K_{RS} factor.

$$X_{\sigma r\_SC} = X_{leak\_airgap} + X_{end\_ring} + X_{slot\_leak\_DC} + X_{leak,incl\_r}. \quad (5)$$

D. SC machine concept: rotor resistance

The typical *E-J* characteristic of HTS materials is depicted in Fig. 2. Its analytical formulation, that is, the power law, at constant temperature and magnetic field is reported in (6). In this equation, E_{hts} is the electric field measured within the superconductor, E_0 is the characteristic electric field, J_{hts} is the operating electric current density, J_c is the critical current density and n is the index value [22]. For the BSCCO-2223 HTS tapes considered in this work, the value for the parameters was $E_0 = 1$ μV/cm, $J_c = 4 \cdot 10^8$ A/m^2 and $n = 30$ [23].

$$E_{hts} = E_0 \cdot \left|\frac{J_{hts}}{J_c(B,T)}\right|^n. \quad (6)$$

The equivalent circuit of the SC machine concept was solved through an iterative procedure because of the nonlinear resistivity (*E-J* characteristic) of the SCs.

Figure 5 illustrates all the steps necessary to solve the equivalent circuit. First, the stator voltage was applied. The initial value for the equivalent rotor-phase resistance R'_{r0} corresponded to the one of the CRYO machine concept. This allowed for a faster convergence of the implemented algorithm.

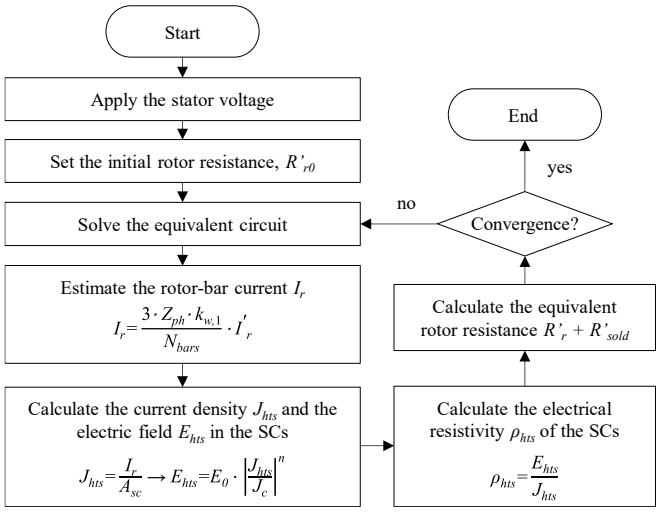

Fig. 5. Flowchart illustrating the iterative procedure carried out for solving the nonlinear equivalent circuit of the SC machine concept.

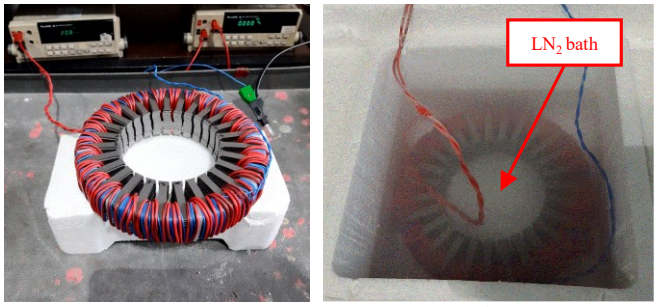

(a) (b)

Fig. 6. The laminated M400-50A grade stator stack used for the characterization of the iron losses at room and cryogenic temperature. (a) Room temperature test at 18 °C. (b) Cryogenic temperature test at -196 °C.

The value for the rotor current I_r was computed by solving the equivalent circuit in Fig. 4b. The current density J_{hts} in the SCs was derived using the cross-sectional area A_{sc} of the parallel of two tapes and the electric field was determined using the power law reported in (6). By knowing both the electric field E_{hts} and the current density J_{hts}, it was possible to obtain the electrical resistivity ρ_{hts} of the SCs. The same value for J_{hts} was considered for both the SCs in the rotor bars and the end-rings. The equivalent rotor-phase resistance R'_r was determined and the contribution of the soldering resistance R'_{sold} was also included. The process was repeated until reaching the convergence and for the slip values $0 \leq s \leq 1$ to obtain the whole torque versus speed characteristic of the SC machine concept.

IV. Results and Discussion

The methodology described in the previous section was implemented to calculate the steady-state electromechanical characteristics of the three machine concepts REF, CRYO and SC, for both the 15 kW and the 90 W reference motors. The reference air-cooled machines (REF) were characterized by analytical calculations as well as experimentally by performing the no-load and locked-rotor tests, following the procedure reported in the international standards [24].

At the moment, the experimental validation of the analytical results obtained for the CRYO induction machine concept was carried out considering the 90 W reference machine operated in LN_2. The experimental tests on the 15 kW machine, as well as the validation of the superconducting machine concept (SC) for both the reference motors will be part of a future work.

A. Iron Losses of SiFe laminations at cryogenic temperature

The iron losses in the ferromagnetic core of an electrical machine are affected by the operating temperature and it is important to consider their variation when solving the equivalent circuit. For this reason, the core losses of a laminated M400-50A grade stator stack were measured and compared at room temperature (18 °C) and at cryogenic temperature (-196 °C).

Figure 6 shows the laminated stator core under test at (a) room temperature and at (b) cryogenic temperature. The Expanded Polystyrene (EPS) foam container was filled with LN_2 to perform the cryogenic test at -196 °C.

The characterization of the iron losses was performed following the procedure described in [25]. The results at a supply frequency of 50 Hz and up to $B_{pk} = 1.7$ T are shown in Fig. 7. The iron losses at cryogenic temperature were higher compared to those at room temperature.

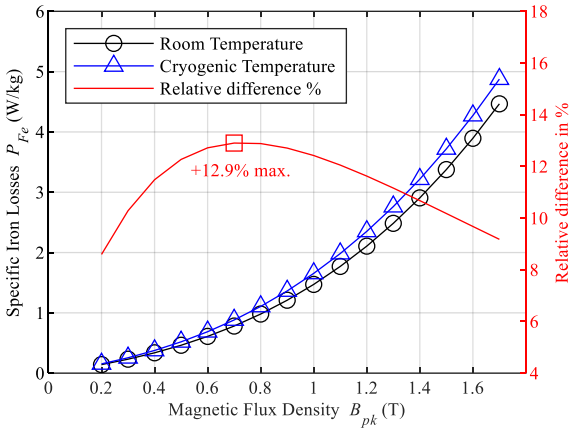

Fig. 7. The specific iron losses at 50 Hz of the laminated M400-50A grade stator stack at room and cryogenic temperature as a function of the peak magnetic flux density.

As a first approximation, the hysteresis loss contribution was considered constant with the temperature. This means that the increase of the core losses was mainly caused by an increase in the dynamic loss components [26]. Indeed, both the eddy current and the excess losses depend on the conductivity of the laminations which increases with lowering the temperature. Figure 7 also reveals that the largest increase of ~ 13% in the iron losses occurred at 0.7 T. Within the range $B = 1.2 \div 1.6$ T an average 10% increase was observed. The value for the iron loss resistance R_{Fe} in the equivalent circuit can be calculated from the conventional iron losses P_{Fe}, determined by the no-load test, and from E_s, the total phase emf induced in the stator winding:

$$R_{Fe} = \frac{3E_s^2}{P_{Fe}}. \tag{7}$$

Considering that the typical values for the magnetic flux density in the core of induction machines are within the range $B = 1.2 \div 1.5$ T, a 10% increase of the iron losses at cryogenic temperature implied a 10% decrease of the iron loss resistance R_{Fe} to be used in the equivalent circuit. Finally, it should be remarked that both the 15 kW and the 90 W machine are manufactured with an M400-50A grade laminated core.

B. Experimental tests on the 90 W reference machine

The methodology proposed in Section III was validated experimentally by testing the 90 W air-cooled machine under cryogenic conditions. Therefore, a comparison between the REF and CRYO machine concepts was carried out. The test setup is shown in Fig. 8. The no-load, the locked-rotor and the load tests were performed under sinusoidal supply at 50 Hz, with the motor operating in air and submerged in LN_2. A DC machine rated 240 W was used as load. The experiments at cryogenic temperature were performed by keeping the machine inside an EPS foam container filled completely with LN_2. The grease of the shaft bearings was removed using acetone. This prevented the failure of the bearings at cryogenic temperature.

Table III reports the parameters of the single-phase equivalent circuit obtained from the experimental tests. The stator and the rotor resistances decreased dramatically because of the operation of the machine submerged in LN_2 at -196 °C.

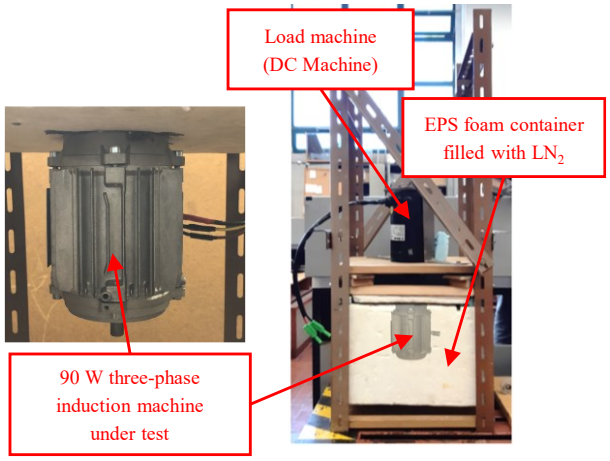

Fig. 8. The experimental setup developed to perform the room temperature and the cryogenic temperature tests on the 90 W machine. During the cryogenic test, the motor was placed into the EPS container and completely submerged by LN_2.

TABLE III. PARAMETERS OF THE SINGLE-PHASE EQUIVALENT CIRCUIT OF THE 90 W MACHINE CONCEPTS FROM THE EXPERIMENTAL TESTS.

Parameters	REF	CRYO	Percentage difference
Stator Resistance, R_s	1.10 Ω	0.20 Ω	-81%
Stator Leakage Reactance, $X_{\sigma s}$	0.53 Ω	0.56 Ω	+4.5%
Eq. Iron loss Resistance, R_{Fe}	116 Ω	97.6 Ω	-16%
Magnetizing reactance, X_m	7.33 Ω	6.97 Ω	-4.9%
Rotor-Phase Resistance R'_r	0.91 Ω	0.22 Ω	-75%
Rotor Leakage Reactance, $X'_{\sigma r}$	0.53 Ω	0.56 Ω	+4.5%

A reduction of the equivalent iron loss resistance revealed the increase of the iron losses in the core at the cryogenic temperature. This 16% decrease was in good accordance with the 10% decrease expected in the range $B = 1.2 \div 1.5$ T as described in Section IV.A. The total leakage reactance obtained from the locked-rotor tests was considered equally split between the stator and the rotor. Their values do not vary significantly when operating in air and at cryogenic temperature, even considering the influence of the skin-effect.

Table IV reports the performance parameters of the three machine concepts simulated at their best efficiency point. The mechanical losses were not included in this analysis. The CRYO machine reached an almost doubled output torque at a higher speed (smaller slip value) and exhibited a better efficiency. The SC machine concept allowed a further 35% increase in torque with respect to CRYO. Moreover, that torque was reached at a rotating speed very close to the synchronous one. The iron losses were calculated considering a 10% increase of the iron loss resistance in the equivalent circuit. Different iron losses were due to a different induced emf E_s on the stator.

Figure 9 compares the performance of the three machine concepts REF, CRYO and SC. The analytical calculations agreed well with the experiments on the REF and CRYO machines. At their best efficiency point, the torque increased from 0.678 Nm to 1.41 Nm. The correspondent maximum efficiency increased of ~ 19% from 0.64 to 0.83. This is mainly due to the remarkable reduction of the copper losses on the stator. Figure 9a illustrates that in the CRYO machine concept, the variation of the resistivity greatly affected the peak value of the torque and its behavior over the whole speed range. The value for the starting torque was also affected.

TABLE IV. CALCULATED PERFORMANCE PARAMETERS AND LOSSES OF THE 90 W MACHINE CONCEPTS AT THEIR BEST EFFICIENCY POINT.

Performance parameters	REF	CRYO	SC
Speed (rpm)	1335	1461	~ 1500
Stator Current (A)	3.3	5.1	6.5
Torque (Nm)	0.66	1.38	1.88
Efficiency	0.625	0.88	0.906
Output Power (W)	92.5	210.9	294.8
Total losses (W)	55.4	28.6	30.7
Stator copper losses (W)	34.1	12.3	20.1
Rotor copper losses (W)	11.5	5.6	10^{-4}
Core losses (W)	9.8	10.7	10.6

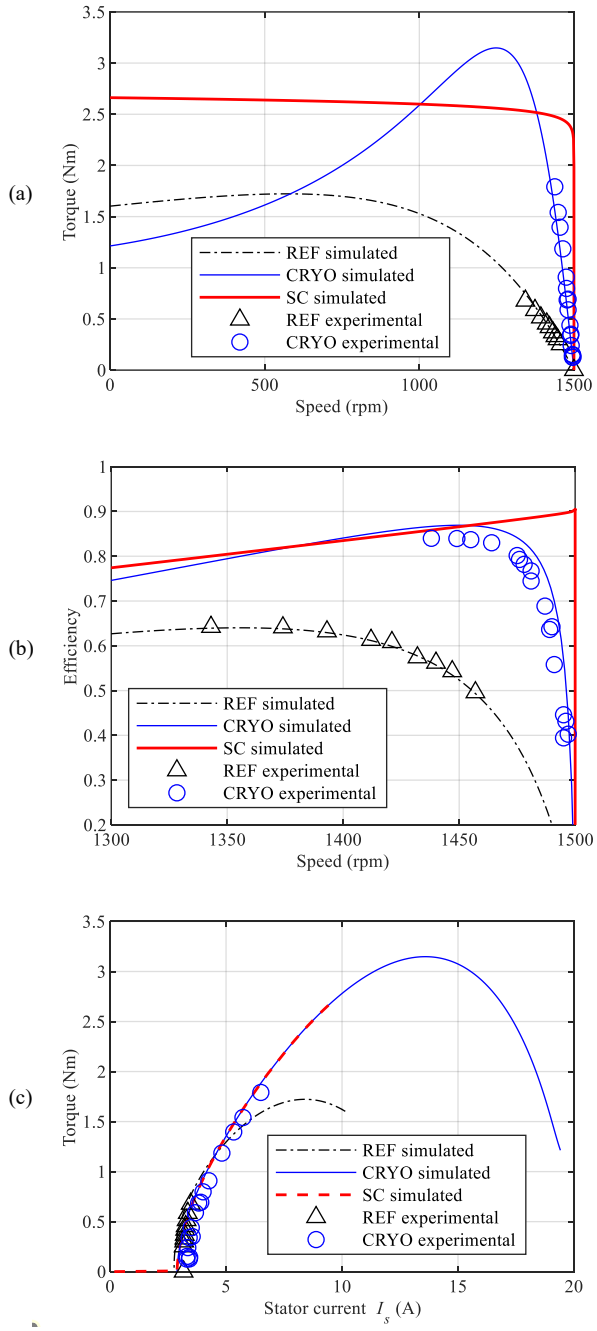

Fig. 9. The performance characteristics of the 90 W air-cooled (REF), cryogenic-cooled (CRYO) and superconducting (SC) machine concepts. (a) Torque vs. speed, (b) Efficiency vs. speed and (c) Torque vs. stator current.

The SC machine concept exhibited a unique behavior of the torque versus speed characteristic. This was because of the nonlinear resistivity of the SCs on the rotor cage. Approaching the synchronous speed, an almost vertical characteristic was due to the very small value for the rotor resistance. In that case, the SCs operated in their superconducting state. As a result, the main contribution to the rotor resistance was represented by R'_{sold}. The torque versus speed behavior of the machine was consistent with the one presented in [15].

Figure 9b demonstrates that the efficiency improvement for both the CRYO and the SC machine concepts was remarkable, especially at low-medium torque values.

Figure 9c shows that all the machines '*use*' the current in the same way for producing the torque.

The power losses in the superconducting cage of the SC machine were computed using the classical formulation for Joule losses, i.e., $P_{Jr} = 3 \cdot R'_r \cdot (I'_r)^2$. Indeed, when rotating almost at the synchronous speed, the frequency of the electrical quantities on the rotor was extremely low. Thus, the *ac* loss phenomena in the superconducting BSCCO-2223 tapes were neglected.

C. *Analytical results on the 15 kW reference machine*

The analytical results on the 15 kW air-cooled machine under cryogenic operation and using a superconducting rotor cage are summarized in Table V and Fig. 10. The results are analogous to those obtained for the 90 W machine. However, in this case, the torque and the efficiency improvement for the CRYO and the SC machine concepts were smaller. In detail, at the best efficiency point, the 90 W machine achieved a remarkable +110% improvement in torque when operating with a cryogenic cooling and a further +36% improvement when employing the superconducting rotor cage. On the other hand, the 15 kW machine achieved a +82% improvement considering the cryogenic cooling and a further +28% improvement with the superconducting rotor cage. Regarding the efficiency, the largest relative improvement was obtained with the cryogenic cooling, for both the 90 W and the 15 kW machines. Therefore, the gain in using SCs seems limited. However, it must be remarked that the machine concepts were compared at a different torque in Table IV and Table V. Conversely, from Fig. 9 and Fig. 10 one can see that, at small slip values (low-medium torque levels), the SC machines exhibited clear advantages in terms of efficiency. This is particularly true for the 90 W SC machine concept.

The torque versus speed characteristic of the 15 kW CRYO machine concept was greatly affected by the different operating temperature, as depicted in Fig. 10a. Of course, the design of the rotor slots was not optimized for an operation at a very low temperature. Indeed, a large temperature gradient does not only influence the *dc* value of the resistivity of the rotor cage, but it also affects the role of the skin effect. The same considerations apply to the efficiency versus speed curve depicted in Fig. 10b, below approximately 1440 rpm.

V. Conclusion

This paper compared the steady-state performances of air-cooled, cryogenic-cooled and superconducting induction machines. Two three-phase industrial motors rated 90 W and 15 kW were taken as the reference for the study. The operation of the machines was analyzed analytically using the single-phase equivalent circuit.

TABLE V. Calculated Performance Parameters and Losses of the 15 kW Machine Concepts at their Best Efficiency Point.

Performance parameters	REF	CRYO	SC
Speed (rpm)	1467	1488	~ 1500
Stator Current (A)	17.2	29.1	37.7
Torque (Nm)	104.3	189.5	242.3
Efficiency	0.923	0.971	0.98
Output Power (kW)	16.02	29.5	38.1
Total losses (W)	1299	875	778
Stator copper losses (W)	599	210	352
Rotor copper losses (W)	320	238	0.04
Core losses (W)	380	427	426

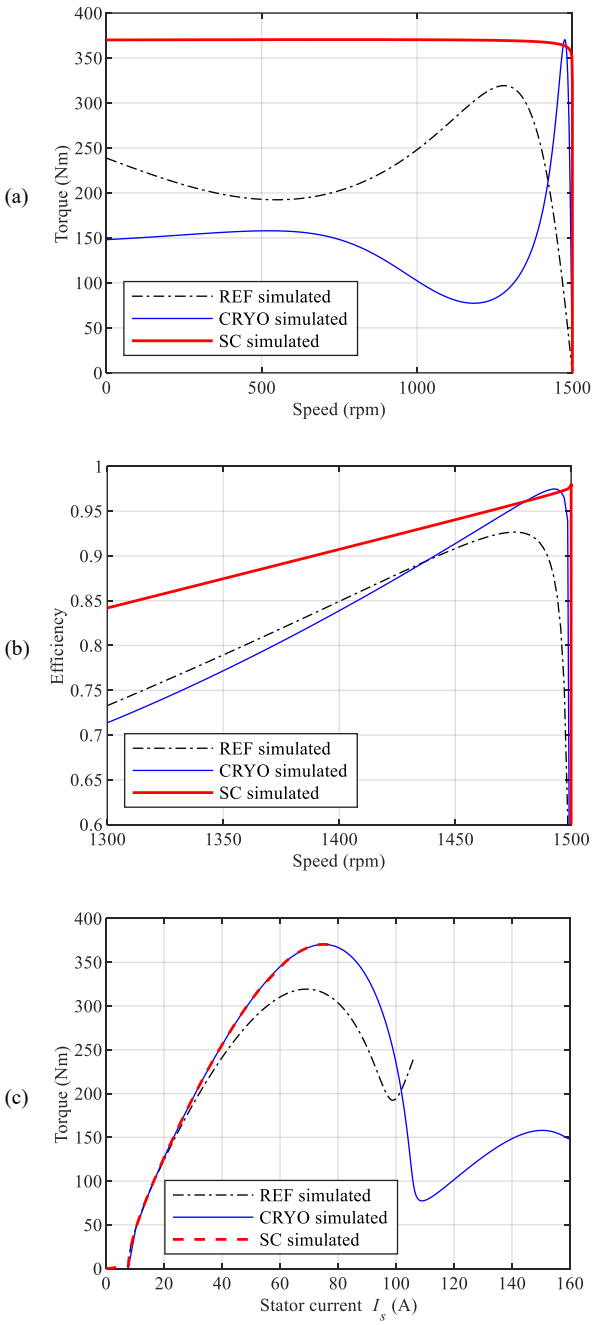

Fig. 10. The performance characteristics of the 15 kW air-cooled (REF), cryogenic-cooled (CRYO) and superconducting (SC) machine concepts. (a) Torque vs. speed, (b) Efficiency vs. speed and (c) Torque vs. stator current.

The methodology proposed to solve the equivalent circuit considered the influence of the temperature and the skin-effect on the machine parameters. The nonlinear resistivity of SCs was considered in the computations by developing a simple iterative procedure to solve the circuit. The simulation results highlighted the remarkable increase in terms of output torque and efficiency of cryogenic-cooled and superconducting induction machines. In addition, the latter exhibited a unique electromechanical characteristic because of the peculiar electric behavior of SCs.

The experimental activities focused on (i) validating the proposed methodology on the 90 W machine operated under cryogenic conditions and (ii) investigating the power losses in a ferromagnetic core at the liquid nitrogen temperature.

The result of the tests conducted on the cryogenic-cooled 90 W motor proved the validity of the proposed approach. The characterization of the core losses demonstrated the increase expected at cryogenic temperature and allowed to include their contribution in the analytical calculations.

At the moment, the testing of the 90 W machine with a superconducting rotor cage as well as the experimental tests on the 15 kW machine were not possible because of the limited facilities available in the lab.

Future research activities will focus on the experimental validation of the SC machine concepts employing the superconducting rotor cage.

ACKNOWLEDGMENT

This work was partially financed by national funds through FCT – Foundation for Science and Technology, I.P., through IDMEC, under LAETA, project UIDB/50022/2020.

REFERENCES

[1] J. H. Redmond, and F. W. Bott. "Development of Cryogenic Electric Motors," *SAE Transactions*, vol. 72, 1964.

[2] R. Shively, "Submerged cryogenic motor materials development," in *IEEE Elect. Insul. Mag.*, vol. 19, no. 3, pp. 7-11, May-June 2003.

[3] M. Biasion, J. F. P. Fernandes, S. Vaschetto, A. Cavagnino and A. Tenconi, "Superconductivity and its Application in the Field of Electrical Machines," 2021 IEEE International Electric Machines & Drives Conference (IEMDC), 2021, pp. 1-7.

[4] T. Nakamura et al., "Tremendous Enhancement of Torque Density in HTS Induction/Synchronous Machine for Transportation Equipments," in *IEEE Trans. Appl. Supercond.*, vol. 25, no. 3, pp. 1-4, June 2015.

[5] T. Nakamura et al., "Load Test and Variable Speed Control of a 50-kW-Class Fully Superconducting Induction/Synchronous Motor for Transportation Equipment," in *IEEE Trans. Appl. Supercond.*, vol. 29, no. 5, pp. 1-5, Aug. 2019.

[6] C. Ai, Y. Huang and H. Wang, "Coupled Electromagnetic and Thermal Analysis of a 15kW Cryogenic Induction Motor for Submerged Liquefied Natural Gas Pumps," 2020 23rd International Conference on Electrical Machines and Systems (ICEMS), Hamamatsu, Japan, 2020.

[7] L. Dlugiewicz, J. Kolowrotkiewicz, W. Szelag, M. Baranski and R. Neumann, "Electrical motor for liquid gas pump," International Symposium on Power Electronics, Electrical Drives, Automation and Motion, 2006, SPEEDAM, Taormina, 2006.

[8] H. Brechna and H. Kronig, "Three phase induction motor with a superconductive cage winding," in *IEEE Trans. Magn.*, vol. 15, no. 1, pp. 715-718, January 1979.

[9] T. A. Lipo (1987), "The Potential for High Temperature Superconducting AC and DC Motors," Electric Machines & Power Systems, 13:6, 373-385.

[10] D. Sekiguchi et al., "Trial Test of Fully HTS Induction/Synchronous Machine for Next Generation Electric Vehicle," in *IEEE Trans. Appl. Supercond.*, vol. 22, no. 3, pp. 5200904-5200904, June 2012.

[11] K. Muranaka, T. Nakamura, S. Okajima, T. Ogasa, N. Amemiya and Y. Itoh, "Experimental and Analytical Studies on Variable Speed Control of High-Temperature Superconducting Induction/Synchronous Motor," in *IEEE Trans. Appl. Supercond.*, vol. 26, no. 4, pp. 1-5, June 2016.

[12] H. M. Kim, K. W. Lee, D. G. Kim, J. H. Park and G. S. Park, "Design of Cryogenic Induction Motor Submerged in Liquefied Natural Gas," in *IEEE Trans. Magn.*, vol. 54, no. 3, pp. 1-4, March 2018.

[13] J. Sim, K. Lee, G. Cha and Ji-K. Lee, "Development of a HTS squirrel cage induction motor with HTS rotor bars," in *IEEE Trans. Appl. Supercond.*, vol. 14, no. 2, pp. 916-919, June 2004.

[14] A. Chengliu, H. Yuanfeng and W. Haifeng, "Main losses study of cryogenic induction motor for submerged liquid natural gas pump," 2015 18th International Conference on Electrical Machines and Systems (ICEMS), Pattaya, 2015, pp. 133-136.

[15] G Morita, T. Nakamura and I. Muta, "Theoretical analysis of a YBCO squirrel-cage type induction motor based on an equivalent circuit," in *Supercond. Sci. Technol.*, vol. 19, pp. 473-478, April 2006.

[16] T Nakamura, Y. Ogama, H. Miyake, K. Nagao and T. Nishimura, "Novel rotating characteristic of a squirrel-cage-type HTS induction/synchronous motor," in *Supercond. Sci. Technol.*, vol. 20, pp. 911-918, August 2007.

[17] K Nagao et al., "Development and fundamental characteristics of a YBCO superconducting induction/synchronous motor operated in liquid nitrogen," in *Supercond. Sci. Technol.*, vol. 21, 015022 (5pp), December 2007.

[18] H. Kitano et al., "Controllability of HTS Induction/Synchronous Machine for Variable Speed Control," in *IEEE Trans. Appl. Supercond.*, vol. 23, no. 3, pp. 5202505-5202505, June 2013.

[19] K. Ikeda et al., "Hysteretic Rotating Characteristics of an HTS Induction/Synchronous Motor," in *IEEE Trans. Appl. Supercond*., vol. 27, no. 4, pp. 1-5, June 2017.

[20] A. Boglietti, A. Cavagnino and M. Lazzari, "Computational Algorithms for Induction-Motor Equivalent Circuit Parameter Determination—Part I: Resistances and Leakage Reactances," in *IEEE Trans. Ind. Electron.*, vol. 58, no. 9, pp. 3723-3733, Sept. 2011.

[21] A. Boglietti, A. Cavagnino and M. Lazzari, "Computational Algorithms for Induction Motor Equivalent Circuit Parameter Determination—Part II: Skin Effect and Magnetizing Characteristics," in *IEEE Trans. Ind. Electron.*, vol. 58, no. 9, pp. 3734-3740, Sept. 2011.

[22] R. M. Scanlan, A. P. Malozemoff and D. C. Larbalestier, "Superconducting materials for large scale applications," in *Proc. IEEE*, vol. 92, no. 10, pp. 1639-1654, Oct. 2004.

[23] A. Mourachkine, Room-Temperature Superconductivity, 1st Ed., Cambridge International Science Publishing, 2004.

[24] "IEEE Standard Test Procedure for Polyphase Induction Motors and Generators," in IEEE Std 112-2017 (Revision of IEEE Std 112-2004), vol., no., pp.1-115, 14 Feb. 2018.

[25] M. Cossale, A. Krings, J. Soulard, A. Boglietti and A. Cavagnino, "Practical Investigations on Cobalt–Iron Laminations for Electrical Machines," in *IEEE Trans. Ind. Appl.*, vol. 51, no. 4, pp. 2933-2939, July-Aug. 2015.

[26] Y. Liu, M. Noe, J. Ou, P. Breining, M. Veigel and M. Doppelbauer, "Measurement of Magnetic Materials at Room and Cryogenic Temperature for Their Application to Superconducting Wind Generators," in *IEEE Trans. Appl. Supercond.*, vol. 28, no. 3, pp. 1-6, April 2018.